Growth of ZnSe Nanospirals with Bending Mediated by Lomer–Cottrell Sessile Dislocations through Varying Pressure

ARTICLE *in* CRYSTAL GROWTH & DESIGN · AUGUST 2008

Impact Factor: 4.89 · DOI: 10.1021/cg8005376

3 AUTHORS, INCLUDING:

Lei Jin
Forschungszentrum Jülich
26 PUBLICATIONS **252** CITATIONS
SEE PROFILE

Jianbo Wang
Wuhan University
334 PUBLICATIONS **6,382** CITATIONS
SEE PROFILE

CRYSTAL GROWTH & DESIGN
2008
VOL. 8, NO. 10
3829–3833

Growth of ZnSe Nanospirals with Bending Mediated by Lomer−Cottrell Sessile Dislocations through Varying Pressure

Lei Jin,[†,‡,§] Jianbo Wang,*[,†,‡] and Wallace C. H. Choy*[,§]

Department of Physics and Center for Electron Microscopy, Wuhan University, Wuhan 430072, China, Key Laboratory of Acoustic and Photonic Materials and Devices of Ministry of Education, Wuhan University, Wuhan 430072, China, and Department of Electrical and Electronic Engineering, University of Hong Kong, Pokfulam Road, Hong Kong, China

Received May 21, 2008; Revised Manuscript Received July 2, 2008

ABSTRACT: ZnSe nanospirals, with zinc blende structured building blocks exhibiting unconventional mosaic configuration, were successfully fabricated via a two-stage growth process, in which abrupt variation of reaction pressure was introduced. In-plane bending, with remarkable morphological difference from the commonly reported nanorings or nanohelixes induced by spontaneous polarization in II−VI semiconductors, has been observed, which can be mainly attributed to existence of numerous Lomer−Cottrell sessile dislocations with edge components. Investigations on morphological evolutions by applying different reaction pressure and growth time in the second stage imply that the formation of nanospirals is closely related to the pressure variation. The results may provide useful information for further understanding the strain release mechanism and mechanical response of ZnSe at the nanoscale.

1. Introduction

ZnSe is one of the key materials for applications in short-wavelength optoelectronic devices and has been highlighted as an efficient emitter[1,2] because of its high quantum yields and proper band gap in the visible region (2.7 eV at 300 K[3]). Zinc blende structured ZnSe had been studied and used in making light-emitting devices and laser diodes in the 1990s.[1,2] Recently, due to the novel properties and promising applications of nanostructures, scientific interests have been renewed for fabricating various ZnSe nanostructures, as well as achieving well-defined interfaces. Different morphologies[4−7] and ZnSe-based nanostructures[8] have been obtained by utilizing various growth techniques, such as metal−organic chemical vapor deposition,[9] molecular beam epitaxy,[10] thermal evaporation,[4,6−8] etc. Among most of these, fabrications are through a one-stage process, since the experimental conditions are maintained throughout the growth. For example, using the thermal evaporation method, pressure-controlled syntheses of ZnSe nanowires and nanorings can be separately achieved.[7]

In contrast to the one-stage syntheses, two-stage fabrications are generally accompanied by variations (i.e., compositions, temperature, and reaction pressure) and thus offer more flexibility in combining different materials and allow separate controls over each material in the single stage. Novel {113} twinned ZnSe bicrystal nanobelts filled with ⟨111⟩ twinnings[11] and side-by-side ZnSe/ZnCdSe bicrystalline nanoribbons[12] have been successfully synthesized through this method. However, reports on the two-stage fabrication of one-dimensional (1D) nanostructures are relatively limited. This may be related to the difficulty of growth during the second stage, such as selection of nucleation sites, lattice matching between different components, and so on.

On the other hand, with the emergence of new directions in flexible dimensionality of electronic devices and forms,[13] as well as the advancements in single nanowire electronics,[14] it has become imperative to investigate the mechanical properties of materials, that is, at the nanoscale. Actually, with the reduction in dimensionality, nanostructures exhibit unique mechanical behavior, which has been demonstrated in various nanostructures.[15,16] Carbon nanotube sheets with tunable Poisson's ratio from positive to negative have been synthesized,[15] and a large strain plasticity of ceramic SiC nanowire at nearly room temperature has been directly observed *in situ* by a high-resolution transmission electron microscopy (HRTEM) technique.[16]

In this paper, we report on the unconventional growth of 1D ZnSe nanospirals via a two-stage fabrication process in which different reaction pressures are applied. The morphological and structural characterizations are performed in section 3.1, which shows that ZnSe nanospirals with novel mosaic blocks compartmentalized by planar defects are obtained. The formation of nanospirals is discussed in section 3.2, which can be attributed to the existence of Lomer−Cottrell sessile dislocations. Evolutions of the ZnSe nanospirals are also investigated in section 3.3, which indicates that the nanospirals form mainly due to the variation of reaction pressure. Finally, some conclusions are drawn in section 4. The results may provide useful information for further understanding the mechanical response of ZnSe at the nanoscale.

2. Experimental Section

2.1. Synthesis. The ZnSe nanospirals were grown in a tube furnace. About 0.5 g of ZnSe powder (99.99% Sigma Aldrich) was loaded in an alumina boat and pushed into the center of the furnace. The silicon (100) substrate, sputtered with ∼20 s of gold film, was placed 30 cm downstream from the source. The furnace was then pumped to ∼0.07 Torr and purged with the carrier gas of highly purified argon premixed with 5% hydrogen at a stable rate of about 200 sccm (sccm denotes standard cubic centimeters per minute) to remove the residual oxygen. After that the flow rate of the carrier gas was maintained at 200 sccm, and the furnace was heated to 950 °C for the subsequent growth.

The growth process was divided into two stages: in the first stage, the reaction pressure was set at 100 Torr and maintained for 35 min; in the second stage, the reaction pressure was changed immediately to 1.5 Torr and maintained for 25 min. After the growth, the furnace was

* To whom correspondence should be addressed. E-mail addresses: wang@whu.edu.cn; chchoy@eee.hku.hk.
† Department of Physics and Center for Electron Microscopy, Wuhan University.
‡ Key Laboratory of Acoustic and Photonic Materials and Devices of Ministry of Education, Wuhan University.
§ Department of Electrical and Electronic Engineering, University of Hong Kong.

10.1021/cg8005376 CCC: $40.75
Published on Web 08/22/2008

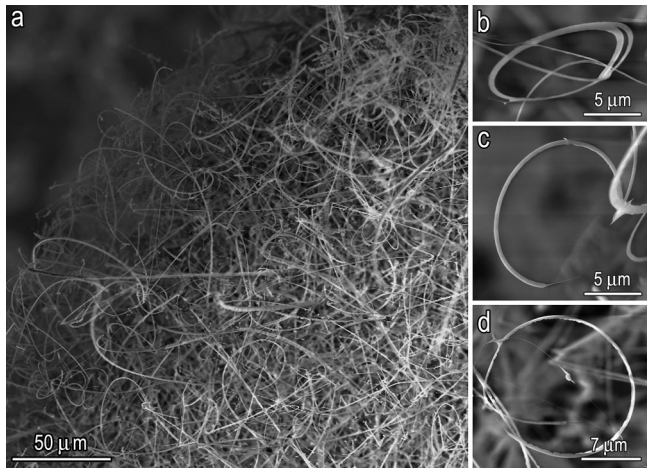

Figure 1. SEM images of (a) the ZnSe nanospirals and (b−d) magnified images showing the typical nanospirals with fully and partially looped morphologies.

cooled naturally to room temperature. Yellowish products were obtained on the substrate.

2.2. Characterization. A LEO-1530 field emission gun scanning electron microscope (SEM) was used for morphological analysis as overall information. The products were then scratched off the substrate and sonicated in ethanol, then dropped onto the holey carbon-coated copper grid for transmission electron microscopy (TEM) observation. TEM observations including bright field (BF) imaging, selected area electron diffraction (SAED) and energy-dispersive X-ray spectroscopy (EDS) were performed using FEI Tecnai G2 20 S-TWIN and JEOL JEM-2010(HT) electron microscopes; HRTEM characterizations were taken on JEOL JEM-2010FEF(UHR) electron microscope equipped with field emission gun and Ω-type in-column energy filter system. All microscopes were operated with the acceleration voltage of 200 kV.

3. Results and Discussion

3.1. Microstructure of ZnSe Nanospirals. The morphology of the as-fabricated nanostructures is investigated by SEM for overall information. It is interesting to observe that the products are bent into spiral-like shapes, with diameters of several tens of micrometers, as shown in Figure 1a. Three representative nanospirals are also presented in the magnified SEM images, as shown in Figure 1b−d. Both fully and partially looped nanospirals can be observed. Moreover, the nanospiral with a larger diameter, such as in Figure 1d, has a relatively rougher inner side surface than those with smaller sizes (Figure 1b,c).

Detailed structural and chemical composition analyses of the products are further carried out using TEM and EDS. Due to their large sizes, the nanostructures are easily damaged resulting in belt-like pieces during the TEM sample preparation process. Shown in Figure 2a is the BF image of a typical fraction. The curved shape reconfirms the nanospiral morphology as observed in Figure 1. The corresponding SAED pattern is also presented in the inset of Figure 2a, which can be attributed to a superimposition of two sets of SAED patterns along $[01\bar{1}]$ and $[0\bar{1}1]$ zone axes of a zinc blende structure (JCPDS 80-0021) and exhibits a $\langle 111\rangle$ twinning-like diffraction pattern.[11] The spots marked by the dashed frame (denoted by footnote T) originate from the $[01\bar{1}]$ zone axis and those marked by solid frame from the $[0\bar{1}1]$ axis. Further investigations show that the [111] axes are always pointing to the center of the nanospiral and the angle between $(\bar{1}11)$ and $(\bar{1}11)_T$ planes is about 141.2°, which is consistent with the previous studies on $\langle 111\rangle$ twinnings of ZnSe.[11] A zoomed-in BF image is shown in Figure 2b; numerous blocks are observed, which constitute the nanospirals.

Assuming that the nanospiral is bent into a circular arc, its radius of curvature may be estimated by shape fitting. Figure 2a,c shows examples of curve fittings; the dashed arcs are superimposed on the nanospirals, with the radii of ∼9 and ∼15 μm, respectively. Similar trend can be observed that the larger the diameters, the rougher the inner side surface. EDS analysis (Figure 2d) indicates that the nanostructures are solely composed of Zn and Se atoms, with a Zn/Se atomic ratio of about 1:1.

For better understanding the microstructures of the novel spirals, thus investigating the formation mechanism, HRTEM images from a large spiral are obtained. Figure 3a represents the BF image and the corresponding schematic illustration, which is constructed based on the outer arc of 21 μm in diameter and fits well to the experimental observation. The area marked by the black frame is further magnified and shown in Figure 3b, which can be simply separated into two regions as indicated by I and II. In comparison with the previously reported ZnSe nanosaws,[17] one striking feature is that an uncommonly mosaic configuration is observed, which occupies more than half of the sample area. Shown in Figure 3c is the HRTEM image from several mosaic blocks, which is recorded from the area labeled by the white frame and projected along $[0\bar{1}1]$ axis. The (111) crystal planes in each block are parallel with respect to each other, which results in a coincidence of the (111) spots in the SAED pattern (inset of Figure 2a). The growth direction of ZnSe nanospirals is along $\langle\bar{2}11\rangle$ axis and changes gradually around the arc. In contrast to the structurally perfect blocks, the HRTEM image indicates that regions sandwiched between blocks are rich in planar defects, that is, stacking faults in {111} planes as indexed in Figure 3c, which are suggested by the stretching of SAED spots in Figure 2a. However, due to the strong delocalization effect, the detailed interfacial structures are barely discernible.

Therefore, HRTEM images from another nanospiral with a lower defect density are shown in Figure 4, from which the interfacial structures have been investigated. Stacking faults in the (111) and $(\bar{1}11)$ planes can be directly observed in Figure 4a and form the acute and obtuse parallel pairs. According to the previous studies, Lomer−Cottrell sessile dislocations (stair−rod partial dislocations) will form and thus bound the stacking faults.[18] The Fourier filtered image from the square enclosed area using spatial frequency as $(\bar{1}11)$ is also inset in Figure 4a, which clearly exhibits the extra half atomic plane. It is noted that the Lomer−Cottrell partial dislocation with different configurations such as Z-shaped faulted dipoles,[19−21] stacking fault pyramids, and trapezoids,[22] has been commonly observed in most face-centered cubic metals[19] and semiconductors[20−22] and may greatly influence the mechanical[18] and optical properties.[22] Moreover, an HRTEM image from the type II region is also shown in Figure 4b. Closer examination indicates that the stacking fault is intrinsic with the displacement $R = -(1/3)\langle\bar{1}11\rangle$ and the bounding Shockley partial dislocation[18] with Burgers vector **b** of $(1/6)\langle 2\bar{1}\bar{1}\rangle$ glides outside the tooth.

3.2. Formation of Nanospirals with in-Plane Bending Mediated by Lomor−Cottrell Sessile Dislocations. In the literature, coiled and zigzag structures have been extensively reported for several materials;[23−34] several mechanisms have also been proposed to interpret the formations.[24−27,29−34] Among the materials, ZnO has been most commonly studied. Various coiled nanostructures induced by spontaneous polarization have been successfully obtained and explained by Wang's group.[30−32] Following a similar explanation, wurtzite ZnSe nanorings have

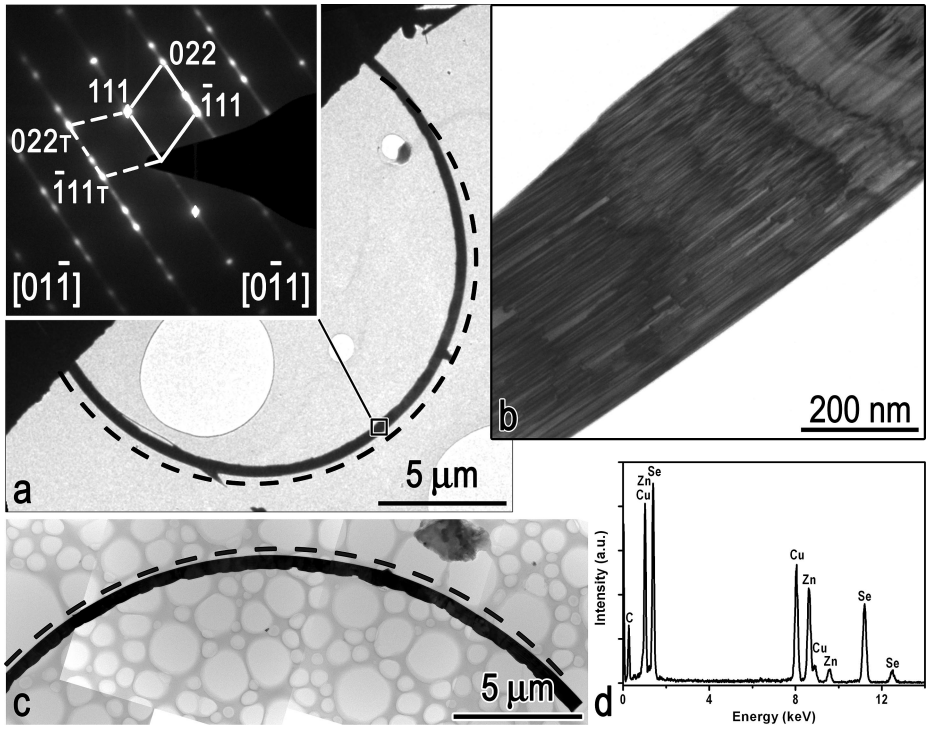

Figure 2. (a) BF image and (b) zoomed-in BF image of a nanospiral with radius of ~9 μm; the inset is corresponding SAED pattern from the marked area. (c) BF image of another nanospiral with radius of ~15 μm. Dashed arcs are superimposed to fit the radii of curvature of nanospirals, respectively. (d) EDS spectrum of panel a.

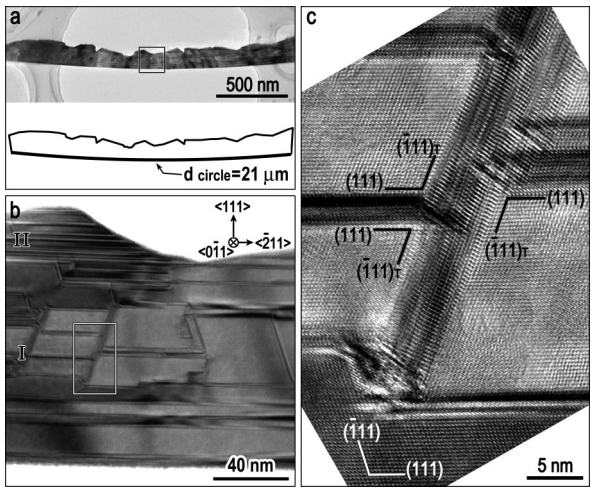

Figure 3. (a) BF and (b) magnified BF TEM images of a nanosprial and (c) corresponding HRTEM image exhibiting unconventional mosaic configuration.

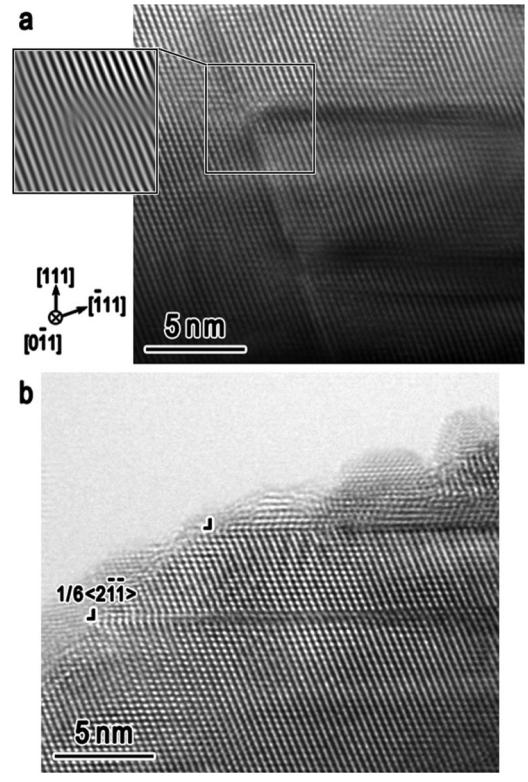

Figure 4. HRTEM images from (a) type I and (b) type II regions of another nanospiral with relatively lower density of defects. The inset is the Fourier filtered image from the square enclosed area using spatial frequency as ($\bar{1}$11) showing the extra half atomic plane.

been synthesized by Leung et al., with dominant {0001} polar surfaces exposed.[7] However, this mechanism relies crucially on the existence of a large polar surface and is obviously not applicable to the as-grown samples here, since the dominant surfaces are nonpolar $\pm(0\bar{1}1)$. Screw dislocations have also been introduced to explain the formation of helical β-Ga_2O_3 nanowires[33] and SiC/SiO_2 core−shell nanowires.[34] However, due to the significant difference in morphology, the nanospirals may not be the case either.

Hence, based on the experimental settings (section 2) and structural analyses (section 3.1), the formation mechanism of the unconventional nanospirals is now discussed, with schematic illustrations as shown in Figure 5. Initially, ZnSe nanobelt forms (Figure 5a) through a two-dimensional growth: growth along [$\bar{2}$11] direction in competition with the self-catalyzed[35] laminar growth toward [111] direction. Such competition, combined with the pressure varying during the growth process, results in the

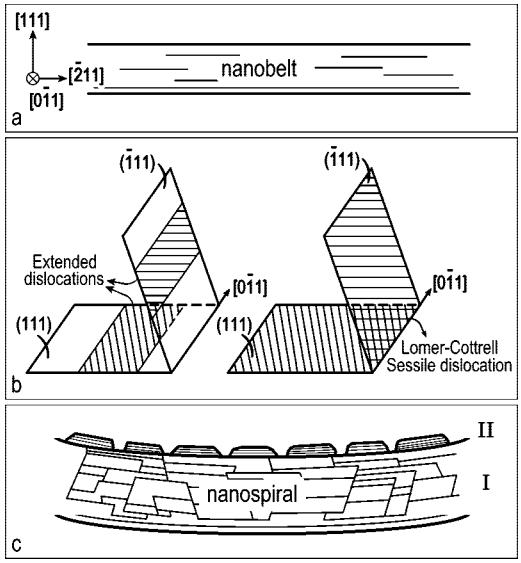

Figure 5. Schematic illustrations demonstrating the formation of in-plane bending: (a) formation of nanobelt concluding extended dislocations; (b) representative process showing the formation of Lomer−Cottrell sessile dislocation; (c) the final morphology of the nanospiral.

Table 1. Reaction Pressures and Corresponding Growth Times before (Stage 1) and after (Stage 2) Variations for Samples A−F

sample	stage 1	stage 2
A	100 Torr (35 min)	
B	100 Torr (35 min)	50 Torr (25 min)
C	100 Torr (35 min)	10 Torr (25 min)
D	100 Torr (35 min)	1.5 Torr (5 min)
E	100 Torr (35 min)	1.5 Torr (15 min)
F	100 Torr (35 min)	1.5 Torr (25 min)

multiplication of dislocations in order to release the local strain. Considering the low stacking fault energy of ZnSe (∼13 mJ m^{-2} at room temperature[36]), perfect dislocation is easily dissociated into two Shockley partial dislocations and a stacking-fault ribbon (so-called extended dislocation)[18] as denoted by the thin line in Figure 5a. In addition, the emergence of stacking faults will further reduce the energy barrier, thus lead to the fastest growth along the direction parallel to the stacking faults.[37]

Meanwhile, extended dislocations in $(\bar{1}11)$ planes simultaneously form and further glide in their own slip planes. Once two stacking faults meet at the line of intersection of two adjacent {111} planes, Lomer−Cottrell partial dislocation will form along one of the six ⟨011⟩ directions, with b of (1/6)⟨011⟩ and thus act as a strong barrier to the glide of further dislocations on the {111} planes. A representative process is demonstrated in Figure 5b, with the dislocation reaction given by eq 1.

$$(1/6)[\bar{1}2\bar{1}] + (1/6)[1\bar{1}2] \rightarrow (1/6)[011] \qquad (1)$$

Using the b^2 criterion for dislocation energy per unit length, the energy after the reaction described by eq 1 exhibits a considerable reduction in comparison with that before the reaction. As the growth proceeds, more and more Lomer−Cottrell partial dislocations form. Due to the immobility of the Lomer−Cottrell partial dislocations of the edge characteristic, the as-grown nanobelt will gradually bend into spiral-like morphology and further maintain this unrecoverable deformation, as illustrated by region I in Figure 5c.

In the later stage, due to the decreasing of the source vapor at local regions, the dominated role of the laminar growth will be replaced by the island growth along [111] direction, thereby

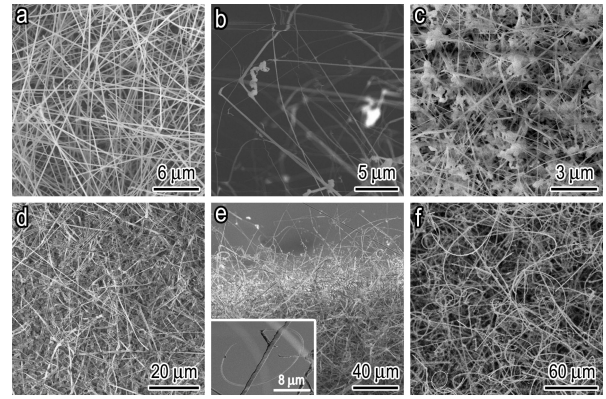

Figure 6. SEM images of the as-synthesized nanostructures showing the morphological evolutions: panels a−f correspond to the morphology of samples A−F, respectively.

resulting in the formation of the tooth-like structures, as denoted by region II in Figure 5c. The Shockley partial dislocations will glide outside the sawteeth, leaving the stacking faults as observed in Figure 4b. One the other hand, by carefully examining our SEM results, we find that spirals with a nearly flat inner side surface are mainly concentrated in the upward area of the substrate, where the ZnSe source vapor is considered to be much denser and the growth is more rapid. Thereby, the teeth regions are relatively smaller and the configuration of mosaic blocks are much compact, which is consistent with the SEM and TEM observations as in section 3.1.

After submission, we also noted that a just-published interesting paper (published May 23, published online May 1, 2008) had also addressed the role of dislocation with screw component in the formation of hierarchical nanostructures.[38] However, we emphasize here that the edge component of dislocation (locked Lomer−Cottrell dislocation) brings about the in-plane bending of nanostructures. Actually, both reports are separate discoveries revealing the two aspects of dislocation mechanism in the growth of nanostructures, just like two sides of a coin.

3.3. Evolution of ZnSe Nanospirals by Varying Reaction Pressure and Growth Time. According to the aforementioned results, ZnSe nanospirals with zinc blende structure can be obtained under the present conditions. However, one question arises: what is the driving force (or key factor) for the formation of nanospirals. Thus, the growth process has been studied by applying different reaction pressures and growth times in the second stage to investigate the morphological evolution of the ZnSe nanospirals. Experimental parameters are listed in detail in Table 1.

The morphologies of samples A−F are shown in Figure 6a−f, respectively. As observed in Figure 6a, uniform nanowires are obtained, which are used as the starting point for the second stage of the growth. After the first stage of the growth, the reaction pressure is changed immediately to 50, 10, and 1.5 Torr; different morphologies are observed in Figure 6b,c,f, respectively. However, only in sample F are nanospirals observed, which implies that the nanospirals will form under a critical pressure below 10 Torr. Actually, when the reaction pressure is changed to ∼5 Torr, nanospirals can also be obtained (not shown).

On the other hand, the morphological evolution of the ZnSe nanospirals is also investigated by changing the growth time from 5 to 25 min in the second stage, while the reaction pressure is maintained at 1.5 Torr. It is found that when the growth time increases to 15 min, several nanospirals form, which is

confirmed by the SEM observations in Figure 6e and the corresponding inset. Thereafter, large quantities of nanospirals begin to grow and finally form the morphologies as observed in Figures 1a and 6f.

4. Conclusions

By utilizing a two-stage method with varying reaction pressure, ZnSe nanospirals with zinc blende structure have been successfully fabricated. Novel mosaic configuration composed of numerous structurally perfect zinc blende blocks has been observed. According to the structural analyses, a dislocation-mediated bending model is proposed to explain the formation mechanism of nanospirals. The morphological evolutions are also investigated, which imply that the formation of nanospirals is closely related to the variation of reaction pressure. This method provides an effective route to fabricate novel structures as well as to further study the mechanical response of ZnSe nanostructures.

Acknowledgment. This work was supported by the Natural Science Foundation for the Outstanding Young Scientists of Hubei Province, China (Grant No. 2005ABB014) and the Program for New Century Excellent Talents in University (NCET). W.C.H. Choy acknowledges the support by the University Development Fund (UDF) and the seed funding of the University of Hong Kong. Yee P. Leung is acknowledged for his technical assistant and useful discussions.

References

(1) Haase, M. A.; Qiu, J.; Depuydt, J. M.; Cheng, H. *Appl. Phys. Lett.* **1991**, *59*, 1272–1274.
(2) Yasuda, T.; Mitsuishi, I.; Kukimoto, H. *Appl. Phys. Lett.* **1988**, *52*, 57–59.
(3) Rujkorakarn, R.; Nelson, A. J. *J. Appl. Phys.* **2000**, *87*, 8557–8560.
(4) Li, Q.; Gong, X. G.; Wang, C. R.; Wang, J.; Ip, K.; Hark, S. K. *Adv. Mater.* **2004**, *16*, 1436–1440.
(5) Hu, Z. D.; Duan, X. F.; Gao, M.; Chen, Q.; Peng, L. M. *J. Phys. Chem. C* **2007**, *111*, 2987–2991.
(6) Liu, S. Y.; Choy, W. C. H.; Jin, L.; Leung, Y. P.; Zheng, G. P.; Wang, J. B.; Soh, A. K. *J. Phys. Chem. C* **2007**, *111*, 9055–9059.
(7) Leung, Y. P.; Choy, W. C. H.; Markov, I.; Pang, G. K. H.; Ong, H. C.; Yuk, T. I. *Appl. Phys. Lett.* **2006**, *88*, 183110.
(8) Wang, C. R.; Wang, J.; Li, Q.; Yi, G. C. *Adv. Funct. Mater.* **2005**, *15*, 1471–1477.
(9) Zhang, X. T.; Liu, Z.; Leung, Y. P.; Li, Q.; Hark, S. K. *Appl. Phys. Lett.* **2003**, *83*, 5533–5535.
(10) Chan, Y. F.; Duan, X. F.; Chan, S. K.; Sou, I. K.; Zhang, X. X.; Wang, N. *Appl. Phys. Lett.* **2003**, *83*, 2665–2667.
(11) Jin, L.; Wang, J. B.; Cao, G. Y.; Xu, Z. L.; Jia, S. F.; Choy, W. C. H.; Leung, Y. P.; Yuk, T. I. *J. Phys. Chem. C* **2008**, *112*, 4903–4907.
(12) Liu, Z.; Shan, C. X.; Hark, S. K.; You, L. P.; Chen, J. *J. Phys. Chem. C* **2007**, *111*, 16181–16183.
(13) Qin, Y.; Wang, X. D.; Wang, Z. L. *Nature* **2008**, *451*, 809–813.
(14) Huang, Y.; Duan, X. F.; Cui, Y.; Lauhon, L. J.; Kim, K.; Lieber, C. M. *Science* **2001**, *294*, 1313–1317.
(15) Hall, L. J.; Coluci, V. R.; Galvão, D. S.; Kozlov, M. E.; Zhang, M.; Dantas, S. O.; Baughman, R. H. *Science* **2008**, *320*, 504–507.
(16) Han, X. D.; Zhang, Y. F.; Zheng, K.; Zhang, X. N.; Zhang, Z.; Hao, Y. J.; Guo, X. Y.; Yuan, J.; Wang, Z. L. *Nano Lett.* **2007**, *7*, 452–457.
(17) Wang, Y. Q.; Philipose, U.; Ruda, H.; Kavanagh, K. L. *J. Mater. Sci.: Mater. Electron.* **2006**, *17*, 1065–1070.
(18) Hull, D.; Bacon, D. J. *Introduction to Dislocations*, 4th ed.; Butterworth-Heinemann: Oxford, U.K., 2001), p 97.
(19) Carter, C. B.; Holmes, S. M. *Philos. Mag.* **1975**, *32*, 599–614.
(20) Spence, J. C. H.; Kolar, H. *Philos. Mag. A* **1979**, *39*, 59–63.
(21) Lim, S. H.; Shindo, D.; Yonenaga, I.; Brown, P. D.; Humphreys, C. J. *Phys. Rev. Lett.* **1998**, *81*, 5350–5353.
(22) Wang, N.; Sou, I. K.; Fung, K. K. *J. Appl. Phys.* **1996**, *80*, 5506–5508.
(23) Motojima, S.; Ueno, S.; Hattori, T.; Goto, K. *Appl. Phys. Lett.* **1989**, *54*, 1001–1003.
(24) Suenaga, K.; Zhang, Y.; IIjima, S. *Appl. Phys. Lett.* **2000**, *76*, 1564–1566.
(25) Mcllroy, D. N.; Zhang, D.; Kranov, Y.; Grant Norton, M. *Appl. Phys. Lett.* **2001**, *79*, 1540–1542.
(26) Sone, E. D.; Zubarev, E. R.; Stupp, S. I. *Angew. Chem., Int. Ed.* **2002**, *41*, 1706–1709.
(27) Bae, S. Y.; Lee, J.; Jung, H.; Park, J.; Ahn, J. P. *J. Am. Chem. Soc.* **2005**, *127*, 10802–10803.
(28) Cai, X. M.; Leung, Y. H.; Cheung, K. Y.; Tam, K. H.; Djurišić, A. B.; Xie, M. H.; Chen, H. Y.; Gwo, S. *Nanotechnology* **2006**, *17*, 2330–2333.
(29) Amelinckx, S.; Zhang, X. B.; Bernaerts, D.; Zhang, X. F.; Ivanov, V.; Nagy, J. B. *Science* **1994**, *265*, 635–639.
(30) Kong, X. Y.; Wang, Z. L. *Appl. Phys. Lett.* **2004**, *84*, 975–977.
(31) Gao, P. X.; Wang, Z. L. *Small* **2005**, *1*, 945–949.
(32) Yang, R. S.; Ding, Y.; Wang, Z. L. *Nano Lett.* **2004**, *4*, 1309–1312.
(33) Zhan, J. H.; Bando, Y.; Hu, J. Q.; Xu, F. F.; Golberg, D. *Small* **2005**, *1*, 883–888.
(34) Zhang, H. F.; Wang, C. M.; Wang, L. S. *Nano Lett.* **2002**, *2*, 941–944.
(35) Wang, Z. L.; Kong, X. Y.; Zuo, J. M. *Phys. Rev. Lett.* **2003**, *91*, 185502.
(36) Aristov, V. V.; Zaretskii, A. V.; Osipyan; Yu, A.; Petrenko, V. F.; Strukova, G. K.; Khodos, I. I. *Phys. Status Solidi a* **1983**, *75*, 101–106.
(37) Kong, X. Y.; Ding, Y.; Yang, R. S.; Wang, Z. L. *Science* **2004**, *303*, 1348–1351.
(38) Bierman, M. J.; Albert Lau, Y. K.; Kvit, A. V.; Schmitt, A. L.; Jin, S. *Science* **2008**, *320*, 1060–1063.

CG8005376